Supplementary Information

A Carnitine-based BODIPY Photosensitizer

Contents

1. Experimental Details

1.1. Synthesis

General Aspects

Chemicals and Solvents

Chemicals and solvents were purchased from one of the following providers: Sigma-Aldrich, Alfa Aesar, Carbosynth, Fluka, Fluorochem, Honeywell, Merck, Panreac, Scharlab or TCI. Anhydrous solvents were prepared according to standard methods by distillation over drying agents or via elution through a PureSolv^{TM} column drying system from Innovative Technology, Inc. All other solvents were of HPLC grade and used as provided.

Reactions

Reaction progress was monitored by normal phase thin layer chromatography (TLC) using Merck Silica Gel 60 F254 plates. Chromatograms were visualized using UV light (254 nm or 365 nm).

Microwave irradiation experiments were performed under magnetic stirring with a single-mode Anton Paar Monowave 300 reactor, using standard Pyrex tubes (10 mL) sealed with PTFE-lined rubber septums under the following conditions of temperature and pressure, respectively: 80 – 120 °C, <20 bar.

Purification

Column chromatography was performed on a 971-FP Flash Purification System (Agilent Technologies) using SF Si35 cartridges.

Structural Characterization

^{1}H and ^{13}C NMR spectra were recorded on a Bruker Avance III-400 (400 and 100 MHz, respectively) or a Varian System 500 (500 and 125 MHz, respectively) spectrometer. Chemical shifts are expressed in parts per million (δ scale) downfield from tetramethylsilane and are referenced to residual peaks of the corresponding deuterated NMR solvents. Data are represented as follows: chemical shift, integration, multiplicity (s = singlet, d = doublet, t = triplet, m = multiplet, b = broad), coupling constants in Hz,

and assignment. Proton and carbon assignments are based on gCOSY, gHSQC and gHMBC correlation experiments.

High-resolution mass spectra (HRMS) were recorded on an Agilent 6520 Accurate Mass Q-TOF instrument with an ESI source. Results are expressed as mass/charge (m/z).

Experimental Procedures

Compound **3**

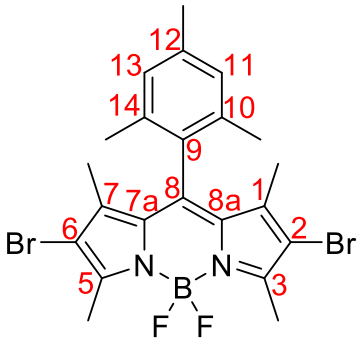

The BODIPY core was halogenated following a known procedure.[1] To a solution of 8-mesityl-1,3,5,7-tetramethyl-4,4-difluoro-4-bora-3a,4a-diaza-s-indacene (75.0 mg, 0.21 mmol, 1.0 eq.) in CH_2Cl_2, *N*-Bromosuccinimide (146 mg, 0.82 mmol, 4.0 eq.) was added and the mixture was stirred at room temperature for an hour before diluting with CH_2Cl_2, washing with a saturated solution of $Na_2S_2O_3$ (20 mL) and extracting with CH_2Cl_2 (2 x 20 mL). The combined organic phases were dried over anhydrous Na_2SO_4, filtered and concentrated at reduced pressure. The crude product was purified by flash chromatography, (SiO_2, hexane → hexane: AcOEt 93:7), yielding compound **3** as an orange solid (104 mg, 0.198 mmol, 97%).

^{1}H NMR ($CDCl_3$, 400 MHz): δ (ppm) = 6.98 (2H, s, H11 and H13), 2.61 (6H, s, $CH_3$3 and $CH_3$5), 2.36 (3H, s, $CH_3$12), 2.07 (6H, s, $CH_3$10 and $CH_3$14), 1.39 (6H, s, $CH_3$1 and $CH_3$7).

^{13}C NMR ($CDCl_3$, 100 MHz): δ (ppm) = 153.7 (C3 and C5), 142.5 (C7a and C8a), 140.0 (C8), 139.4 (C12), 134.9 (C10 and C14), 130.6 (C9), 129.7 (C1 and C7), 129.4 (C11 and C13), 111.5 (C2 and C6), 21.4 ($CH_3$12), 19.6 ($CH_3$10 and $CH_3$14), 13.8 ($CH_3$3 and $CH_3$5), 12.7 ($CH_3$1 and $CH_3$7).

HRMS (ESI$^+$): For $C_{22}H_{24}BBr_2F_2N_2$ $[M+H]^+$, m/z (calc.) = 525.03465; m/z (found) = 525.03753. For $C_{22}H_{23}BBr_2F_2N_2Na$ $[M+Na]^+$, m/z (calc.) = 547.0166; m/z (found) = 547.01824.

Compound **1**

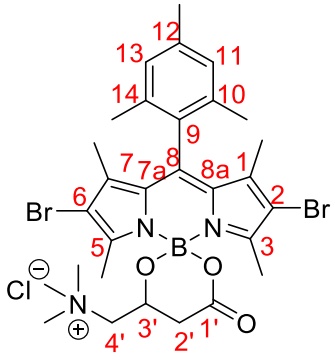

Procedure 1

To a solution of compound **3** (16.0 mg, 31 µmol, 1.2 eq.) and L-carnitine hydrochloride (5.0 mg, 26 µmol, 1.0 eq.) in dry CH_3CN (1.5 mL), TMSCl (163 µL, 1.3 mmol, 51 eq.) was added and the mixture was heated in a microwave reactor (30 min at 80 °C, 30 min at 100 °C and 2h at 120 °C) before being dried at reduced pressure. The crude product was purified by crystallization (CH_2Cl_2/TBME).

Procedure 2

A solution of (*R*)-**BCT-2** (145 mg, 0.28 mmol, 1.0 eq.) in CH_2Cl_2 (5.0 mL) was added to a flask containing *N*-bromosuccinimide (123 mg, 0.68 mmol, 2.5 eq.) and the mixture was stirred at room temperature, in the dark, for 35 minutes. The solvent was evaporated at reduced pressure and the obtained crude product was purified by crystallization (CH_2Cl_2/TBME).

Compound **1** was obtained as a purple solid in a 40% yield (6.9 mg, 0.01 mmol) following procedure 1 and in a 39% yield (73.2 mg, 0.11 mmol) following procedure 2.

^{1}H NMR ($CDCl_3$, 500 MHz): δ (ppm) = 6.99 (1H, s, H11/H13), 6.97 (1H, s, H13/H11), 4.54 (2H, t, *J* = 10.2 Hz, H4'), 4.15 (1H, d, *J* = 13.1 Hz, H3'), 3.29 (9H, s, $(CH_3)_3$N4'), 2.96 (2H, d, *J* = 17.3 Hz, H2'), 2.61 (3H, s, $CH_3$3/ $CH_3$5), 2.46 (3H, s, $CH_3$5/ $CH_3$3), 2.35 (3H, s, $CH_3$12), 2.03 (3H, s, $CH_3$10/ $CH_3$14), 1.96 (3H, m, $CH_3$14/ $CH_3$10), 1.40 (3H, s, $CH_3$7/ $CH_3$1), 1.38 (3H, s, $CH_3$1/ $CH_3$7).

^{13}C NMR ($CDCl_3$, 101 MHz): δ (ppm) = 168.9 (C1'), 154.1 (C3/C5), 152.6 (C5/C3), 143.0 (C8), 141.4 (C8a/C7a), 141.3 (C7a/C8a), 139.9 (C12), 134.9 (C10/C14), 134.0 (C14/C10), 130.6 (C9), 130.4 (C7/C1), 130.4 (C1/C7), 129.8 (C11/C13), 129.6 (C13/C11), 113.2 (C2/C6), 112.9 (C6/C2), 69.2 (C3'), 62.7 (C4'), 54.8 ($(\underline{CH_3})_3$N4'), 36.7 (C2'), 21.4 ($\underline{CH_3}$12), 19.7 ($\underline{CH_3}$10/ $\underline{CH_3}$14), 19.5 ($\underline{CH_3}$14/ $\underline{CH_3}$10), 16.1 ($\underline{CH_3}$5/ $\underline{CH_3}$3), 14.3 ($\underline{CH_3}$3/ $\underline{CH_3}$5), 13.3 ($\underline{CH_3}$7/ $\underline{CH_3}$1), 13.1 ($\underline{CH_3}$1/ $\underline{CH_3}$7).

HRMS (ESI$^+$): For $C_{29}H_{37}BBr_2N_3$ $[M]^+$, m/z (calc.) = 646.1276; m/z (found) = 646.1280.

1.2. Photophysical Characterization

Absorption and Fluorescence Spectra

Absorption spectra were recorded by UV-Vis-NIR Spectroscopy (model Cary 7000, Agilent Technologies, Madrid, Spain) equipped with two lamps (a halogen lamp for the Vis-IR region and a deuterium lamp for the UV region).

Fluorescence measurements were recorded with an Edinburgh Instruments spectrofluorimeter (FLSP920 model, Livingston, UK) equipped with a xenon flash lamp (450 W) as the excitation source. Fluorescence spectra were corrected from the wavelength dependence on the detector sensibility. The fluorescence quantum yields of the photosensitizers were measured by a relative method, using pyrromethene 567 (Φ_{fl} = 0.87 in EtOH) as a standard sample, and applying the following equation to deduce quantum yield values from experimental data:

$$\Phi_{fl} = \Phi_{fl}^{r} \frac{n^2}{(n^r)^2} \frac{F^r}{F} \frac{A}{A^r}$$

where n is the refractive index of the solvent, F is the area under the curve of the emission band and A is the absorbance at the chosen excitation wavelength. Superscript r refers to the known data of the reference sample.

Fluorescence Lifetime

Radiative decay curves were recorded in the same Edinburgh Instruments spectrofluorimeter (FLSP920, Livingston, UK) by Time-Correlated Single-Photon Counting Technique (TC-SPC), using a microchannel plate detector (Hamamatsu C4878) with picoseconds time resolution (≈100 ps). Fluorescence decay curves were monitored at the maximum emission wavelength after excitation using a Fianium super continuous wavelength tunable-laser with 150 ps FWHM pulses.

Fluorescence lifetimes were obtained by studying the evolution of fluorescence intensity with time. Fluorescence intensity for a molecule presenting monoexponential kinetics is described by the following equation:

$$I_{fl}(t) = I_{fl,0} * e^{-t/\tau}$$

where $I_{fl,0}$ = fluorescence intensity immediately after excitation, t = time, and τ = fluorescence lifetime. Upon graphic representation of this equation on a logarithmic scale, fluorescence lifetime can easily be determined from the slope.

$$\ln\left(I_{fl}(t)\right) = \ln\left(I_{fl,0}\right) - \frac{t}{\tau}$$

Phosphorescence

Samples were excited at 500 nm and phosphorescence spectra were recorded at 77 K using an Optisa DN cryostat and ITC601 temperature controller (Oxford Instruments) in a methanol: dichloromethane mixture (1:1).

Singlet Oxygen Quantum Yield

The singlet oxygen quantum yield (Φ_Δ) was determined by direct method measuring its phosphorescence at 1276 nm employing a NIR detector (InGaAs detector, Hamamatsu G8605-23), integrated into the same Edinburgh spectrofluorimeter upon continuous monochromatic excitation (450 W Xenon lamp) of the sample in 1 cm cells in front configuration (front face), 40° and 50° to the excitation and emission beams, respectively, and leaned 30° to the plane formed by the direction of incidence. The value was obtained by the media of at least five different concentrations (range from $2x10^{-6}$

M to 5x10^{-5} M) and using commercial photosensitizer 8-methylthio-2,6-diiodoBODIPY (MeSBDP, CAS-1835282-63-7, Φ_Δ = 0.95 in ACN) as reference.[2]

The experimental determination of Φ_Δ involves the comparison of the signals obtained for each compound to those of a reference with known singlet oxygen quantum yield in the same conditions (solvent, irradiation wavelength and similar absorbance at excitation wavelength). Mathematically, this comparison is represented by the following equation:

$$\Phi_\Delta^{PS} = \Phi_\Delta^R * \frac{S_e^{PS}}{S_e^R}\frac{\alpha^R}{\alpha^{PS}}$$

where Φ_Δ = $^1O_2$ quantum yield, S_e = $^1O_2$ signal intensity at 1276 nm, and α = absorption factor = 1 – 10^{-A}, with A = absorbance at excitation wavelength.

Nanosecond Transient Absorption Spectroscopy

TA spectra in the nanosecond range (ns-TA) and triplet state lifetimes ($^3PS^*$) were recorded in Laser Flash Photolysis (LP980, Edinburgh Instruments). Samples were excited with a computer-controlled Nd:YAG laser coupled to OPO system from LOTIS (TII 2134) operating at 1 Hz and with a pulse width of 7 ns. The transient spectra were registered in spectral mode with ICCD (Andor's iStar DH320T) and the kinetic decay curves in a PMT detector (Hamamatsu R928). Triplet lifetimes were obtained from the corresponding decay of the triplet transient band at the absorption maximum in the presence (aerated solutions) and absence of oxygen (de-aerated solution). Data were analyzed using the LP900 software.

The fractions of triplet excited states quenched by O_2 ($P_{O_2}^T$) were calculated according to the following equation, taking into account the triplet lifetimes obtained in the presence (τ_T) and in the absence of oxygen (τ_T^0):

$$P_{O_2}^T = 1 - \frac{\tau_T}{\tau_0}$$

Rate constants for oxygen quenching of the triplet state (k_{q,O_2}^T) were obtained via the pseudo-first order decay constant of the Stern-Volmer equation:

$$\frac{1}{\tau^T} - \frac{1}{\tau_0^T} = k_{q,O_2}^T[O_2]$$

1.3. Electrochemistry measurements

Electrochemical properties were measured by cyclic voltammetry (Metrohm Autolab) using a three-electrode set up with a platinum disk (diameter 3 mm) working electrode, platinum wire as counter electrode and Ag/AgCl as reference electrode. A 0.1 M solution of tetrabutylammonium hexafluorophosphate (TBAPF6) in dry acetonitrile was used as the electrolyte solvent in which the compounds were dissolved to achieve a concentration of 5 mM. All redox potentials were reported vs ferrocene as internal standard. The solutions were purged with argon and all the measurements were performed under an inert atmosphere.

1.4 Electronic structure calculations

Computational details

Ground state molecular geometries were optimized with the density functional theory (DFT) in combination with the B3LYP exchange-correlation functional and the 6-31+G(d) basis set for all atoms except for Br, for which we used 6-31G(d). Excited state calculations were done within the frame of (linear response) time-dependent DFT (TDDFT) with the CAM-B3LYP energy functional[3] and the cc-pVDZ basis set,[4] as this approach has shown good performance in the study of photophysical properties of BODIPY derivatives.[5] Spin-orbit couplings between singlet and triplet states were evaluated with the same functional and basis set, and by means of the Breit-Pauli Hamiltonian[6] and disregarding two-electron contributions.[7] All electronic structure calculations have been performed with the Q-Chem program.[8]

1.5 Biological Assays

Microscopy and Imaging

The microscope used for the visual analysis of the cells was a Zeiss AxioObserver Z1 wide field inverted fluorescence microscope (Carl Zeiss, Germany) with a Plan-Apochromat 40X/1.3 (NA = 1.3, working distance = 0.21 mm) or Plan-Apochromat 63X/1.4 (NA = 1.4,

working distance = 0.19 mm) oil lens objective, a camera (AxioCam MRm; Carl Zeiss), a CO_2 incubator, and a Zeiss ApoTome.2 structured illumination system. ApoTome.2 allows acquisition of optical sections of the fluorescent sample by moving the appropriate grid into the beam path and calculating the optical section from three images with different grid positions without time lag. Acquisition and processing of images were conducted using the Zen (Carl Zeiss) software. To calculate ROI colocalization values, a standard pixel-wise colocalization analysis was performed, comparing pixel intensities from one channel with corresponding pixels in the second channel of the dual-color image. Within the defined ROI, a scatterplot was generated, and Pearson's correlation coefficient was calculated to quantify the spatial correlation between the two fluorophores.

Cell Viability and Apoptosis Measurements

Irradiation

Cells used in viability and apoptosis assays were irradiated with a LED Par 64 Short Q4-18 (Showtec, Burgebrach, Holland) light-emitting diode device with emission wavelength centered at 518 nm (power: 11.5 mW; fluence rate: 8.6 $mV \cdot cm^{-2}$; dose for 20 min irradiation = 10 $J \cdot cm^{-2}$).

The cytotoxicity of **1** was assessed in SCC42B and SCC38 cells using the MTS (CellTiter 96 Aqueous One, Promega, Madison, WI) and WST-8 cell proliferation assays. Cells were routinely maintained at 37 °C under 5% CO_2 using DMEM media containing 10% fetal bovine serum, **1** and 1% penicillin–streptomycin.

MTS assays

For MTS assays, cells (5000 cells/well) were seeded in a 96-well plate, incubated for 24 h, and treated with varying concentrations in the range of 140 – 1000 nm of **1** or DMSO (0.01%) as vehicle control. After a 30-minute incubation at 37 °C, cells were washed, replenished with DMEM, and incubated for an additional 30 min. Subsequently, cells were either kept in the dark or irradiated with green light for 20 min. After 24 h of incubation with DMEM, 20 µL of CellTiter 96 Aqueous MTS Reagent was added to each well, and absorbance was measured at 490 nm according to the manufacturer's instructions. Cell viability was quantified relative to the DMSO control, correcting for

background absorbance at 492 nm. The assay was performed with four wells per concentration, repeated three times for each cell line.

WST-8 assays

For WST-8 assays, cells (5000 cells/well) were seeded in a 96-well plate, incubated for 24 h, and treated with varying concentrations in the range of 17.5 – 140 nm of **1** or DMSO (0.01%) as vehicle control. After a 30-minute incubation at 37 °C, cells were washed, replenished with DMEM, and incubated for an additional 30 min. Subsequently, cells were either kept in the dark or irradiated with green light for 20 min. After 24 h of incubation with DMEM, 20 µL of WST-8 Reagent was added to each well, and cells were incubated at room temperature in the dark for an hour before absorbance was measured at 460 nm. Cell viability was quantified relative to the DMSO control, correcting for background absorbance at 492 nm. The assay was performed with four wells per concentration, repeated three times for each cell line.

Annexin V/PI apoptosis assays

Cells were seeded in 6-well cell culture plates and on the following day, **1** or DMSO (0.01%) as control was added to each flask. After 30 min incubation, media was withdrawn, and cells were washed, replenished with DMEM, and incubated for an additional 30 min. Subsequently, cells were either kept in the dark or irradiated with green light for 20 min. For determination of apoptosis, cells were trypsinized and collected into FACS tubes. Pellets were washed with PBS and resuspended in 100 µL annexin V buffer (10 mM HEPES pH 7.4, 140 mM NaCl, 2.5 mM $CaCl_2$) and 5 µL annexin V-FITC (BD Bioscience). Immediately prior to analysis, propidium iodide was added. Data were acquired using a FACS Aria IIu (BD biosciences) flow cytometer and analyzed using FlowJo v9.6.2, reporting single- and double-positive populations as apoptotic. The assays were performed with three wells per concentration.

2. Supplementary Figures

2.1. Photophysical characterization

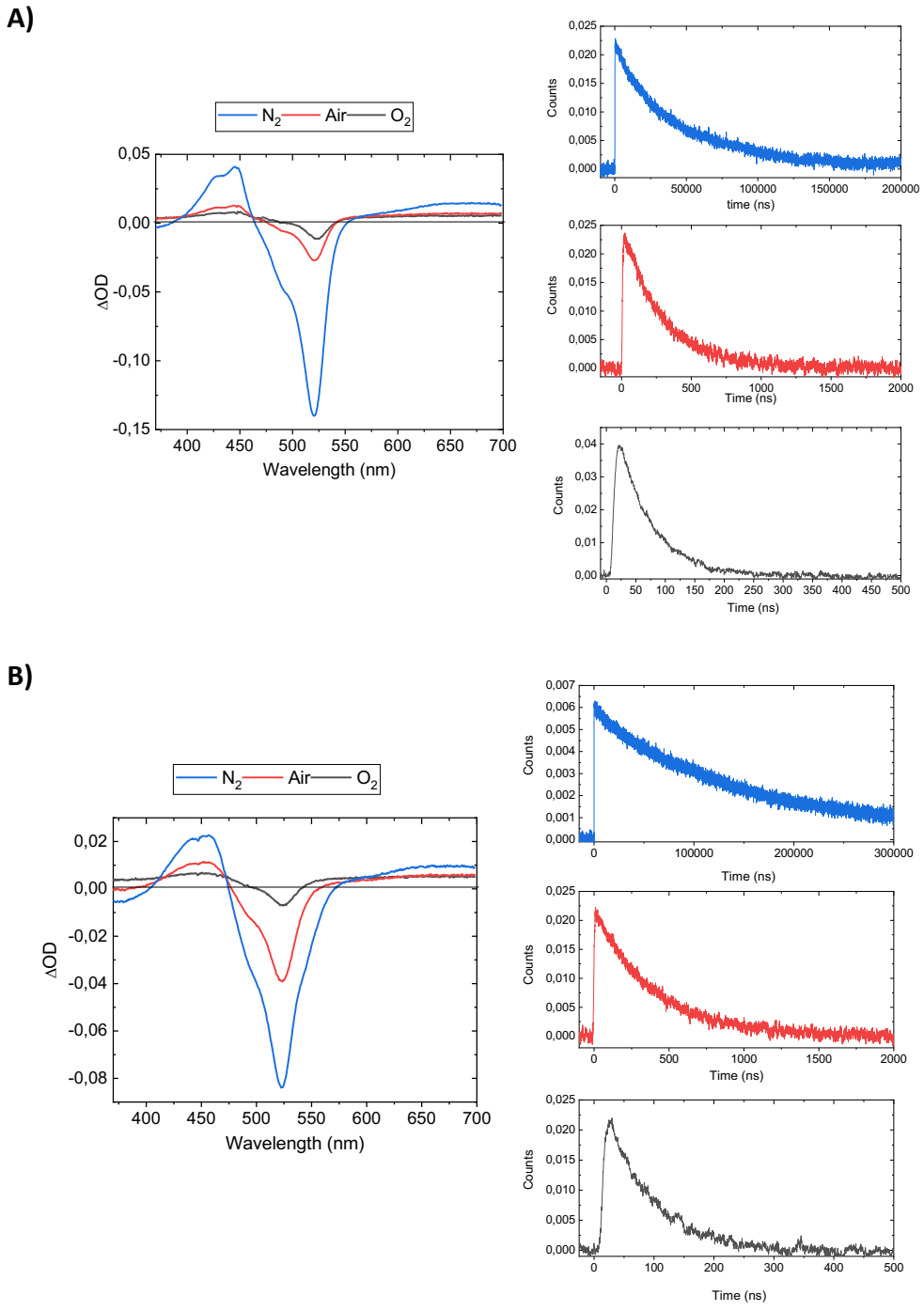

Figure S1. Nanosecond transient absorption spectra and decay curves in acetonitrile upon excitation at 525 nm and saturating the samples in nitrogen, air and oxygen, respectively, for compound **3** (A) and **1** (B).

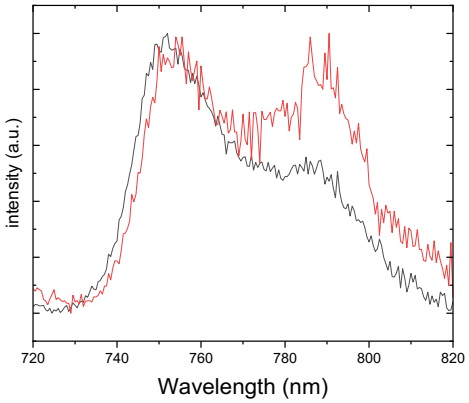

Figure S2. Emission spectra of **3** (top) and **1** (bottom) in a MeOH:CH_2Cl_2 (1:1) mixture at 298 K (red) and 77 K (black), excited at 500 nm.

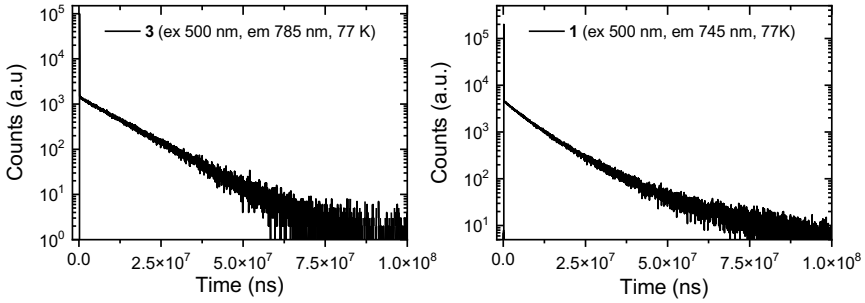

Figure S3. Decay curves of **3** (left) and **1** (right) in MeOH:CH_2Cl_2 (1:1) excited at 500 nm at 77 K.

2.2. Voltammetry

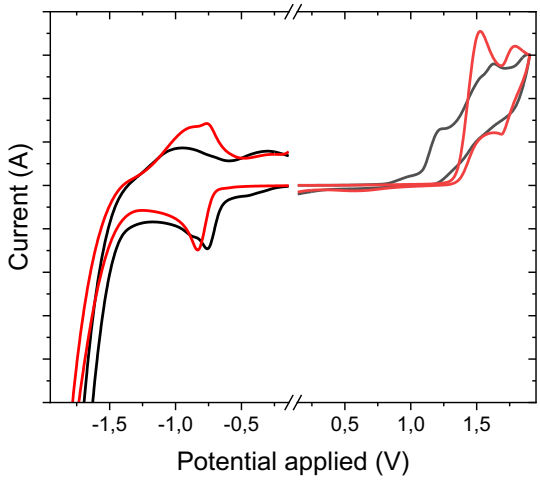

Figure S4. Cyclic voltammograms of BODIPY **3** (black line) and **1** (red line) in concentrated solutions (5 mM) of acetonitrile (0.1 M of TBAPF6), scanned at 0.2 V/s starting in positive direction for oxidation potentials and in negative direction for reduction potentials

2.3. Biological assays

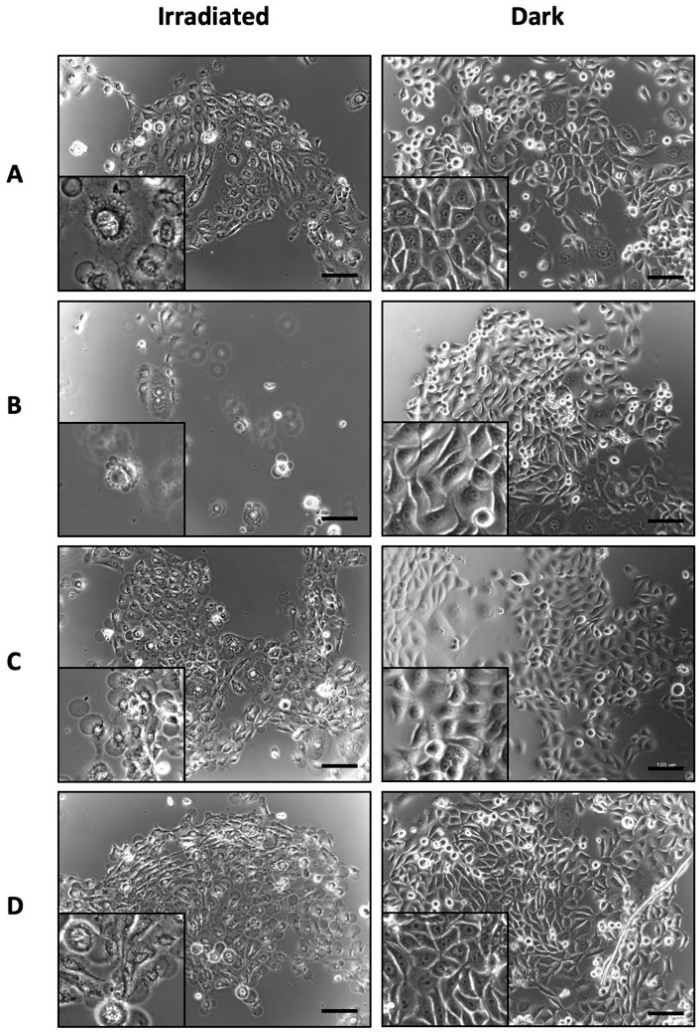

Figure S5. Bright-field images of SCC42B cells treated with different concentrations of probe **1**, under the conditions described in the text. A) 14 μM, B) 7 μM, C) 1.4 μM, D) 0.14 μM.

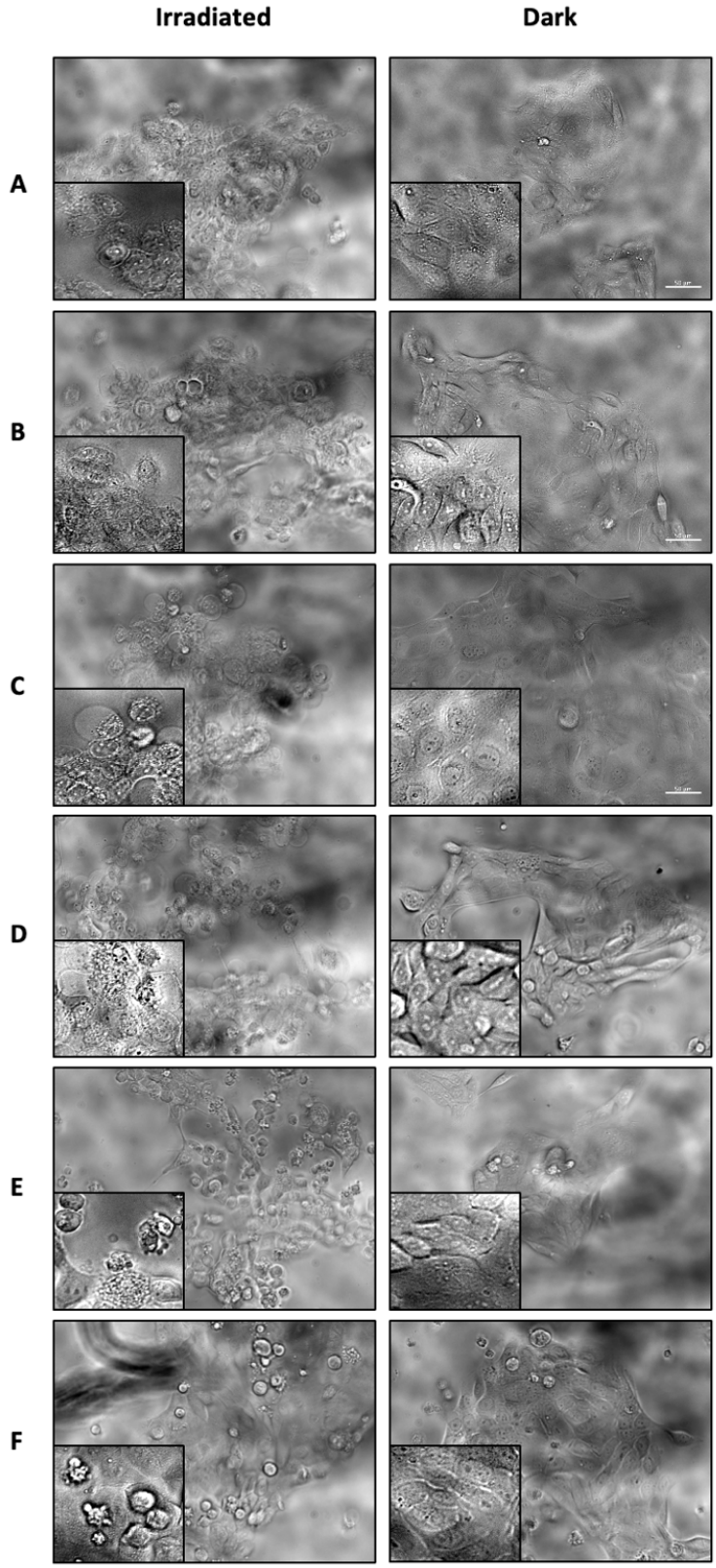

Figure S6. Bright-field images of SCC38 cells treated with different concentrations of probe **1**, under the conditions described in the text. A) 14 μM, B) 7 μM, C) 1.4 μM, D) 0.7 μM, E) 0.14 μM, F) 0.07 μM.

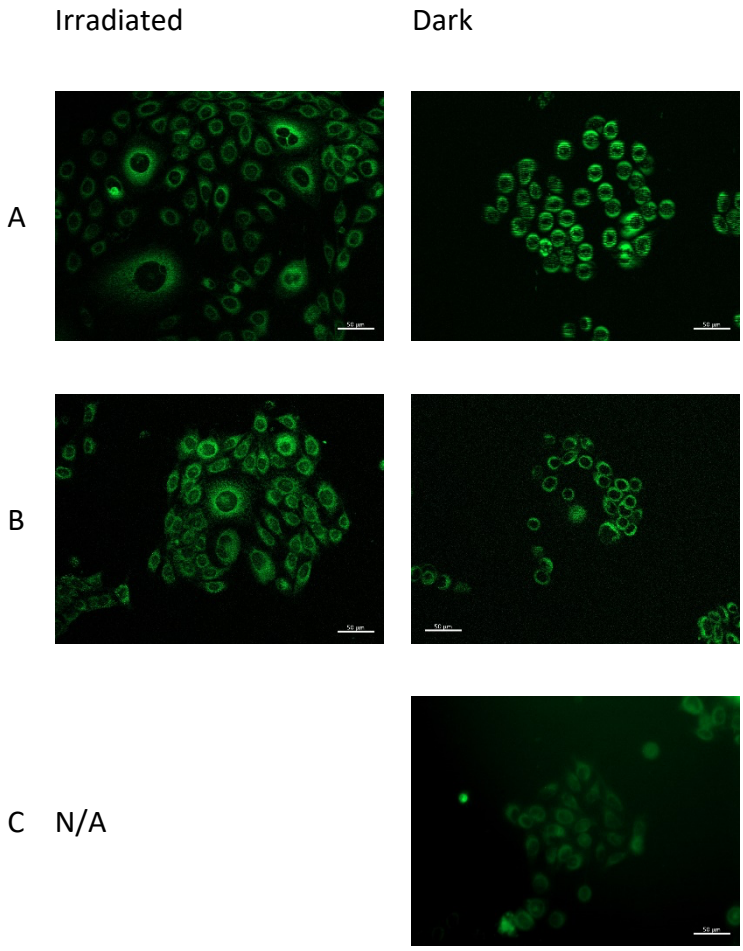

Figure S7. Fluorescence images of SCC42B cells treated with different concentrations of probe **1**. A) 14 µM, B) 7 µM, C) 1.4 µM.

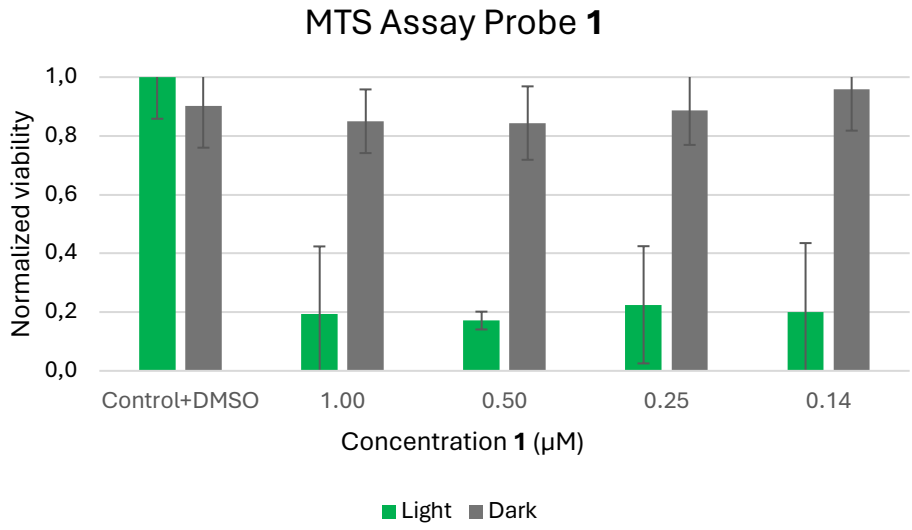

Figure S8. MTS Assay with different concentrations of probe **1** in SCC38 cells.

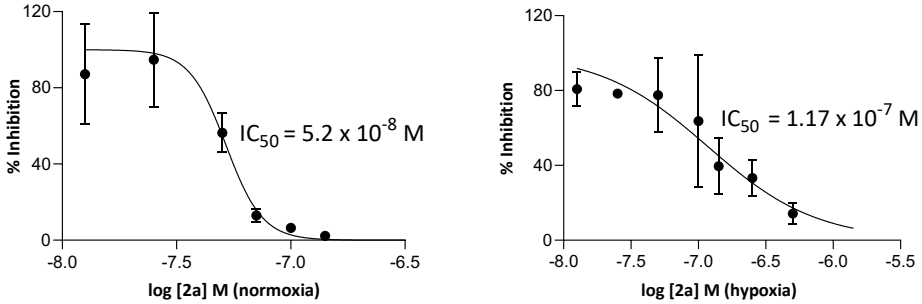

Figure S9. IC_{50} values for probe **1** in normoxia and hypoxia.

2.4. NMR Spectra

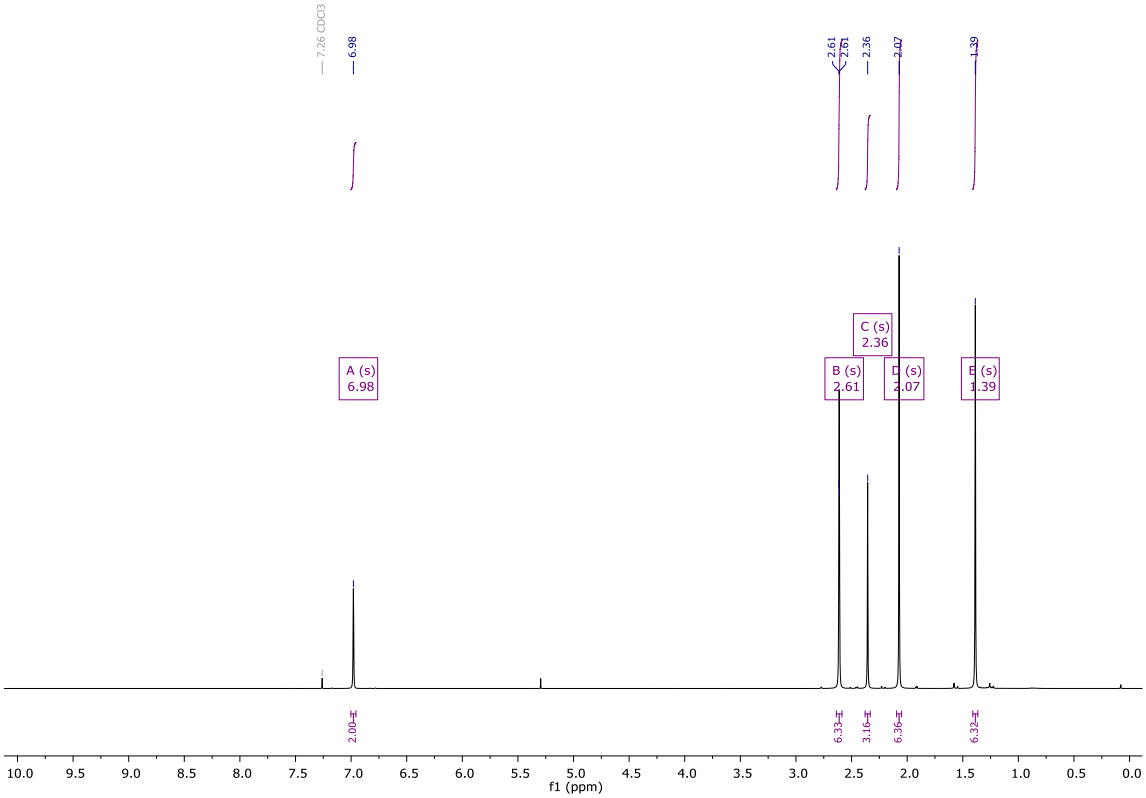

Figure S10. ^1H NMR spectrum ($CDCl_3$, 400 MHz) of compound **3**.

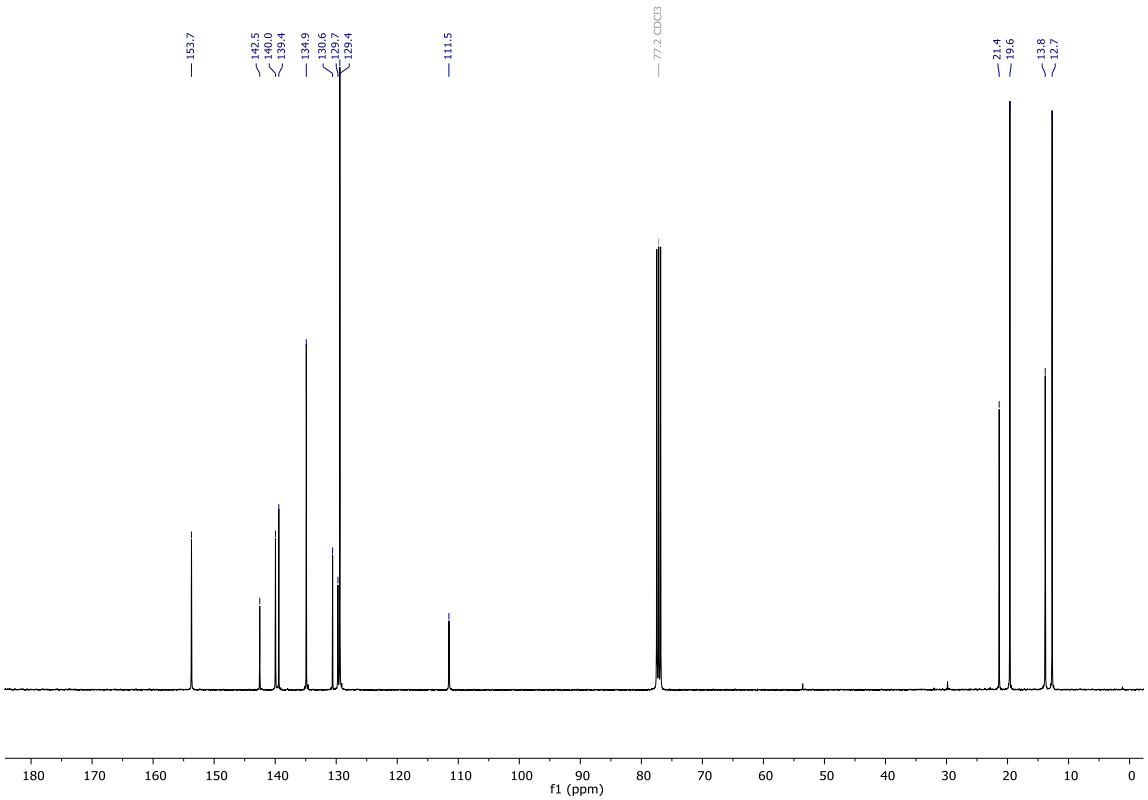

Figure S11. ^{13}C NMR spectrum ($CDCl_3$, 101 MHz) of compound **3**.

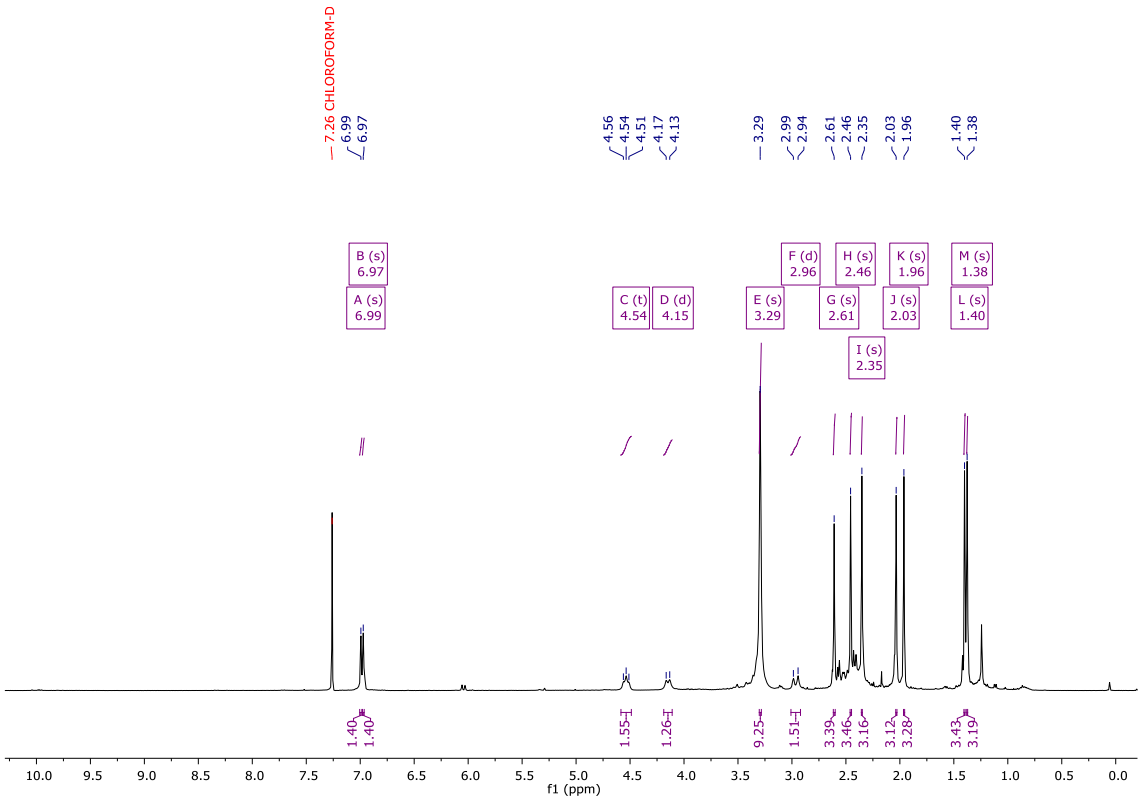

Figure S12. ^{1}H NMR spectrum ($CDCl_3$, 400 MHz) of probe **1**.

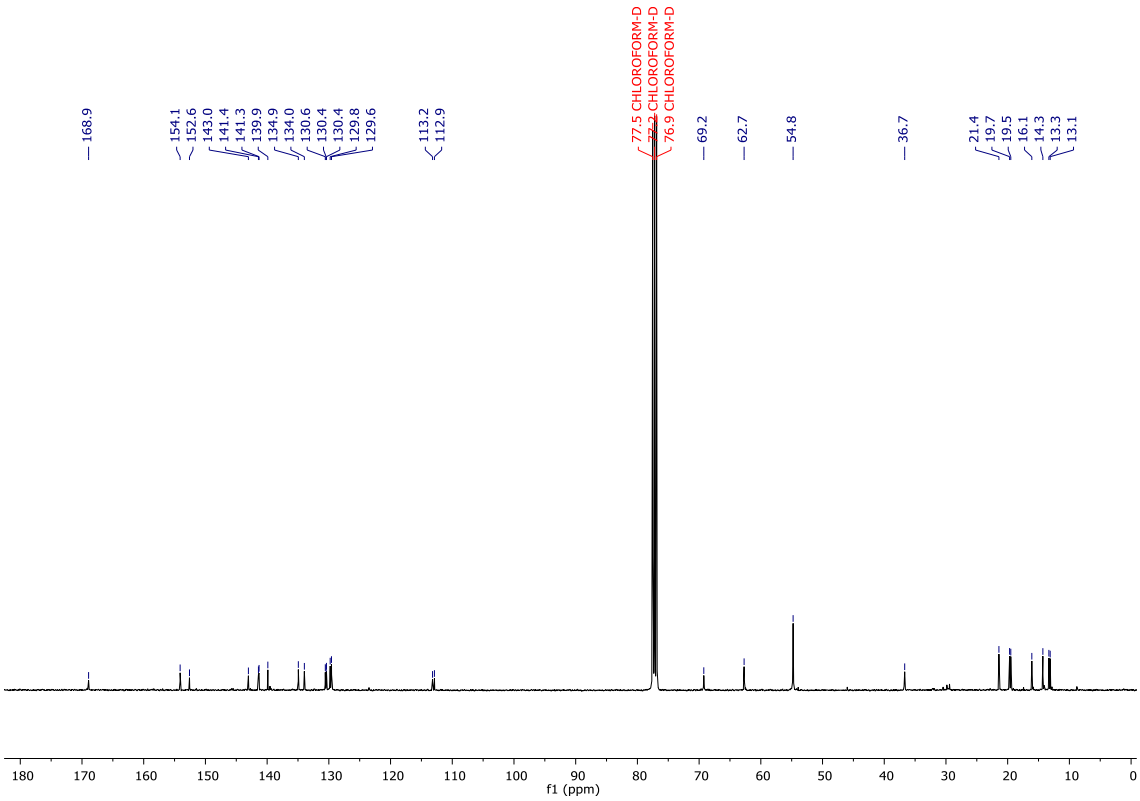

Figure S13. ^{13}C NMR spectrum ($CDCl_3$, 101 MHz) of probe **1**.

3. Supplementary Tables

Table S1. Excitation energies (ΔE in eV), oscillator strengths (*f*) and orbital composition (in %) for the transition to the low-lying excited states of at the ground state geometry of compound **3** computed at CAM-B3LYP/cc-pVDZ level. H_n = HOMO-*n*; L_n = LUMO+*n*.

State	ΔE	*f*	Composition
T_1	1.6426	0.0	$H_0 \rightarrow L_0$ (95%)
T_2	2.8954	0.0	$H_1 \rightarrow L_0$ (87%)
T_3	3.0899	0.0	$H_2 \rightarrow L_0$ (84%) $H_5 \rightarrow L_0$ (7%)
S_1	3.1541	0.7894	$H_0 \rightarrow L_0$ (90%) $H_1 \rightarrow L_0$ (5%)
T_4	3.5812	0.0	$H_0 \rightarrow L_4$ (6%) $H_2 \rightarrow L_0$ (6%) $H_5 \rightarrow L_0$ (78%) $H_{10} \rightarrow L_0$ (5%)
T_5	3.8136	0.0	$H_3 \rightarrow L_0$ (96%)
S_2	3.8446	$2.7 \cdot 10^{-5}$	$H_3 \rightarrow L_0$ (96%)

Table S2. Excitation energies (ΔE in eV), oscillator strengths (*f*) and orbital composition (in %) for the transition to the low-lying excited states of at the ground state geometry of probe **1** computed at CAM-B3LYP/cc-pVDZ level. H_n = HOMO-*n*; L_n = LUMO+*n*.

State	ΔE	*f*	Composition
T_1	1.6564	0.0	$H_o \rightarrow L_o$ (94%)
T_2	2.8537	0.0	$H_1 \rightarrow L_o$ (16%) $H_2 \rightarrow L_o$ (34%) $H_4 \rightarrow L_o$ (33%)
T_3	3.1055	0.0	$H_3 \rightarrow L_o$ (81%)
S_1	3.1092	0.6297	$H_o \rightarrow L_o$ (90%)
T_4	3.5184	0.0	$H_1 \rightarrow L_o$ (67%) $H_2 \rightarrow L_o$ (27%)
S_2	3.5527	$2.9 \cdot 10^{-3}$	$H_1 \rightarrow L_o$ (79%) $H_2 \rightarrow L_o$ (17%)

Table S3. De-excitation energy (ΔE in eV), oscillator strength (*f*) and orbital composition (in %) for the $S_1 \rightarrow S_0$ transition from the S_1 optimized geometry of compound **3** computed at CAM-B3LYP/cc-pVDZ level. H_n = HOMO-*n*; L_n = LUMO+*n*.

State	ΔE	*f*	Composition
S_1	3.0081	0.6527	$L_o \rightarrow H_o$ (89%) $L_o \rightarrow H_1$ (6%)

Table S4. De-excitation energy (ΔE in eV), oscillator strength (*f*) and orbital composition (in %) for the $S_1 \rightarrow S_0$ transition from the S_1 optimized geometry of probe **1** computed at CAM-B3LYP/cc-pVDZ level. H_n = HOMO-*n*; L_n = LUMO+*n*.

State	ΔE	*f*	Composition
S_1	2.9315	0.4953	$L_o \rightarrow H_o$ (89%)

Table S5. Energy gaps ($\Delta E = E(S_1)-E(T_n)$ in eV) and spin-orbit coupling constants (SOCC in cm^{-1}) between S_1 and low-lying triplet states (T_n with n = 1-4) computed at the S_1 optimized geometry of compound **3** computed at CAM-B3LYP/cc-pVDZ level.

State	ΔE	SOCC
T_1	1.4095	0.0262
T_2	0.2407	0.0090
T_3	0.0461	2.7455
T_4	-0.4823	0.4200

Table S6. Energy gaps ($\Delta E = E(S_1)-E(T_n)$ in eV) and spin-orbit coupling constants (SOCC in cm^{-1}) between S_1 and low-lying triplet states (T_n with n = 1-4) computed at the S_1 optimized geometry of probe **1** computed at CAM-B3LYP/cc-pVDZ level.

State	ΔE	SOCC
T_1	1.3394	2.5485
T_2	0.2316	2.0554
T_3	-0.0083	5.1246
T_4	-0.5316	9.8586

4. Supplementary References

1 A. Stafford, D. Ahn, E. K. Raulerson, K.-Y. Chung, K. Sun, D. M. Cadena, E. M. Forrister, S. R. Yost, S. T. Roberts and Z. A. Page, *J. Am. Chem. Soc.*, 2020, **142**, 14733–14742.

2 R. Prieto-Montero, R. Sola-Llano, R. Montero, A. Longarte, T. Arbeloa, I. López-Arbeloa, V. Martínez-Martínez and S. Lacombe, *Phys. Chem. Chem. Phys.*, 2019, **21**, 20403–20414.

3 T. Yanai, D. P. Tew and N. C. Handy, *Chem. Phys. Lett.*, 2004, **393**, 51–57.

4 T. H. Dunning, *J. Chem. Phys.*, 1989, **90**, 1007–1023.

5 R. Prieto-Montero, A. Díaz Andres, A. Prieto-Castañeda, A. Tabero, A. Longarte, A. R. Agarrabeitia, A. Villanueva, M. J. Ortiz, R. Montero, D. Casanova and V. Martínez-Martínez, *J. Mater. Chem. B*, 2023, **11**, 169–179.

6 H. A. Bethe and E. E. Salpeter, *Quantum Mechanics of One- and Two-Electron Atoms*, Springer US, Boston, MA, 1977.

7 Q. Ou and J. E. Subotnik, *J. Phys. Chem. C*, 2013, **117**, 19839–19849.

8 E. Epifanovsky, A. T. B. Gilbert, X. Feng, J. Lee, Y. Mao, N. Mardirossian, P. Pokhilko, A. F. White, M. P. Coons, A. L. Dempwolff, Z. Gan, D. Hait, P. R. Horn, L. D. Jacobson, I. Kaliman, J. Kussmann, A. W. Lange, K. U. Lao, D. S. Levine, J. Liu, S.

C. McKenzie, A. F. Morrison, K. D. Nanda, F. Plasser, D. R. Rehn, M. L. Vidal, Z.-Q. You, Y. Zhu, B. Alam, B. J. Albrecht, A. Aldossary, E. Alguire, J. H. Andersen, V. Athavale, D. Barton, K. Begam, A. Behn, N. Bellonzi, Y. A. Bernard, E. J. Berquist, H. G. A. Burton, A. Carreras, K. Carter-Fenk, R. Chakraborty, A. D. Chien, K. D. Closser, V. Cofer-Shabica, S. Dasgupta, M. de Wergifosse, J. Deng, M. Diedenhofen, H. Do, S. Ehlert, P.-T. Fang, S. Fatehi, Q. Feng, T. Friedhoff, J. Gayvert, Q. Ge, G. Gidofalvi, M. Goldey, J. Gomes, C. E. González-Espinoza, S. Gulania, A. O. Gunina, M. W. D. Hanson-Heine, P. H. P. Harbach, A. Hauser, M. F. Herbst, M. Hernández Vera, M. Hodecker, Z. C. Holden, S. Houck, X. Huang, K. Hui, B. C. Huynh, M. Ivanov, Á. Jász, H. Ji, H. Jiang, B. Kaduk, S. Kähler, K. Khistyaev, J. Kim, G. Kis, P. Klunzinger, Z. Koczor-Benda, J. H. Koh, D. Kosenkov, L. Koulias, T. Kowalczyk, C. M. Krauter, K. Kue, A. Kunitsa, T. Kus, I. Ladjánszki, A. Landau, K. V. Lawler, D. Lefrancois, S. Lehtola, R. R. Li, Y.-P. Li, J. Liang, M. Liebenthal, H.-H. Lin, Y.-S. Lin, F. Liu, K.-Y. Liu, M. Loipersberger, A. Luenser, A. Manjanath, P. Manohar, E. Mansoor, S. F. Manzer, S.-P. Mao, A. V. Marenich, T. Markovich, S. Mason, S. A. Maurer, P. F. McLaughlin, M. F. S. J. Menger, J.-M. Mewes, S. A. Mewes, P. Morgante, J. W. Mullinax, K. J. Oosterbaan, G. Paran, A. C. Paul, S. K. Paul, F. Pavošević, Z. Pei, S. Prager, E. I. Proynov, Á. Rák, E. Ramos-Cordoba, B. Rana, A. E. Rask, A. Rettig, R. M. Richard, F. Rob, E. Rossomme, T. Scheele, M. Scheurer, M. Schneider, N. Sergueev, S. M. Sharada, W. Skomorowski, D. W. Small, C. J. Stein, Y.-C. Su, E. J. Sundstrom, Z. Tao, J. Thirman, G. J. Tornai, T. Tsuchimochi, N. M. Tubman, S. P. Veccham, O. Vydrov, J. Wenzel, J. Witte, A. Yamada, K. Yao, S. Yeganeh, S. R. Yost, A. Zech, I. Y. Zhang, X. Zhang, Y. Zhang, D. Zuev, A. Aspuru-Guzik, A. T. Bell, N. A. Besley, K. B. Bravaya, B. R. Brooks, D. Casanova, J.-D. Chai, S. Coriani, C. J. Cramer, G. Cserey, A. E. DePrince, R. A. DiStasio, A. Dreuw, B. D. Dunietz, T. R. Furlani, W. A. Goddard, S. Hammes-Schiffer, T. Head-Gordon, W. J. Hehre, C.-P. Hsu, T.-C. Jagau, Y. Jung, A. Klamt, J. Kong, D. S. Lambrecht, W. Liang, N. J. Mayhall, C. W. McCurdy, J. B. Neaton, C. Ochsenfeld, J. A. Parkhill, R. Peverati, V. A. Rassolov, Y. Shao, L. V. Slipchenko, T. Stauch, R. P. Steele, J. E. Subotnik, A. J. W. Thom, A. Tkatchenko, D. G. Truhlar, T. Van Voorhis, T. A. Wesolowski, K. B. Whaley, H. L. Woodcock, P. M. Zimmerman, S. Faraji, P. M. W. Gill, M. Head-Gordon, J. M. Herbert and A. I. Krylov, *J. Chem. Phys.*, 2021, **155**, 084801.